Wall-modeled large eddy simulation of shock/turbulent boundary-layer interaction in a duct

I. Bermejo-Moreno, J. Larsson, L. Campo, J. Bodart, Ronan Vicquelin, D. Helmer, J. Eaton

Wall-modeled large eddy simulation of shock/turbulent boundary-layer interaction in a duct

By I. Bermejo-Moreno, J. Larsson, L. Campo, J. Bodart, R. Vicquelin, D. Helmer AND J. Eaton

1. Motivation and objectives

The canonical problem of the interaction of an oblique shock wave impinging upon and reflecting from a turbulent boundary layer (see Fig. 1 for a schematic diagram) has been the focus of extensive research in the fluid dynamics community owing to its relevance in aeronautical engineering applications, ranging from efficient inlet design for air-breathing supersonic engines to fluid-structure interaction and noise reduction in high-speed aircraft. Experiments (see Dolling 2001; Dupont *et al.* 2006, 2008; Humble *et al.* 2009; Souverein *et al.* 2010, and references therein) and numerical simulations, both DNS (Wu & Martin 2008; Pirozzoli & Grasso 2006) and LES (Garnier *et al.* 2002; Touber & Sandham 2009) have greatly increased our understanding of this interaction over the last several decades, but open fundamental questions still remain, such as the origin of large-scale low-frequency motions (Pirozzoli *et al.* 2010) and the effects of three-dimensionality in the flow features (Hadjadj *et al.* 2010), when side walls are present. Numerical simulations are often performed with periodic transverse boundary conditions that simplify the simulation by eliminating two side walls but do not allow a characterization of such 3D effects. Recent experiments performed by Helmer & Eaton (2011) were designed specifically to address this latter issue.

One of the difficulties that arises when comparing experimental results with numerical simulations is that the large Reynolds numbers achieved in the experiments are not reproducible in the simulations because of the prohibitive computational cost that would be required to resolve all the scales present in the flow. Direct numerical simulations (DNS) that resolve all scales are therefore limited to relatively low Reynolds numbers. In large-eddy simulations (LES), a compromise is made to reach higher Reynolds numbers by utilizing a sub-grid scale model for the smaller scales of turbulence motion. But even then, resolving the boundary layer structures that result from the presence of the wall is still too expensive for most flow conditions of practical interest. A further step involves the use of a wall-model, that greatly reduces the computational cost and allows present simulations to reach comparable Reynolds numbers as those found experimentally.

The objective of this study is to perform a wall-modeled large-eddy simulation (WM-LES) of the interaction of an oblique shock and a turbulent boundary layer in a low-aspect-ratio duct that replicates the experimental conditions of Helmer & Eaton (2011), focusing on the effects of three-dimensionality in the flow structure, while evaluating the adequacy of a simple equilibrium wall-model to reproduce the main features observed experimentally. This would allow further exploration of the flow features that may not be retrievable through currently available experimental measurement techniques.

This brief is structured as follows. Section 2 describes the flow conditions and the

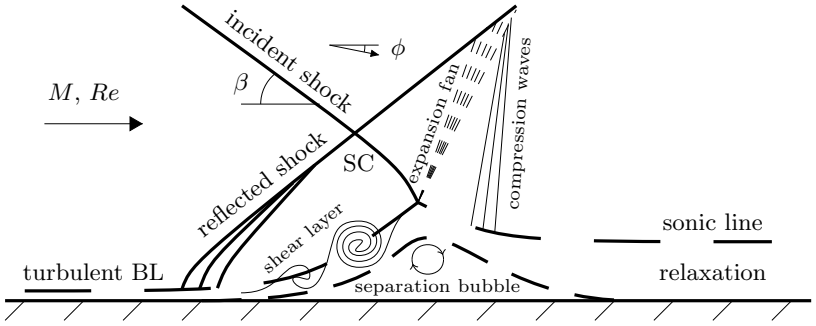

FIGURE 1. Schematic diagram of the shock-turbulent-boundary-layer interaction (adapted from Touber & Sandham 2009). M and Re are the Mach and Reynolds numbers of the incoming flow, respectively; β is the incident shock angle; ϕ is the deflection angle experienced by the flow when traversing the incident shock; SC is the shock-crossing point, defined as the intersection between the incident and reflected shocks. The presence of a separation bubble is dependent on the strengths of the adverse pressure gradient resulting from the interaction and the incoming turbulent boundary layer (TBL).

computational setup utilized to replicate the experiment, as well as the description of the numerical method used to solve the governing equations, with particular emphasis on the wall-model and turbulent inflow. Results of the simulation are presented in section 3 and compared with those obtained in the experiment, emphasizing the three-dimensionality that characterizes this flow. In this regard, the presence of corner flows in the LES is highlighted. Conclusions and future plans are presented in section 4.

2. Flow conditions and computational setup

The computational domain (see Fig. 2) consists of a 118 mm-long rectangular constant-area section of 45.2 mm $\times$ 47.5 mm, followed by a contraction produced by a 20°, 3 mm-long wedge that spans the top wall and is responsible for generating the oblique shock that will impinge and reflect at the bottom wall. Another constant-area section with the new height resulting from the wedge contraction extends 104 mm farther downstream after the wedge.

This domain matches part of the test section of the continuously operated Mach 2.05 wind tunnel used in the experiment (see Helmer & Eaton 2011, for details), which fed from a 2D converging/diverging nozzle and had a longer development section upstream of the wedge and also extended farther downstream before exhausting into a plenum. The turbulent incoming boundary layers had an average thickness of $\delta_0 = 5.4$ mm, measured 21 mm upstream of the foot of the wedge on the top wall. The Reynolds number based on the momentum thickness of the incoming boundary layers at that measurement location was $Re_\theta \approx 6,500$. The velocity at the center line was measured to be 525 m/s.

The numerical code named CharLES, developed at the Center for Turbulence Research, Stanford University, is employed to perform the numerical simulation of this flow. It is a control-volume-based, finite-volume solver of the spatially filtered, compressible Navier-Stokes equations on unstructured grids. It uses a third-order Runge-Kutta time discretization and a grid-based blend of non-dissipative central and dissipative upwind fluxes (see Khalighi *et al.* 2011, for further details on the numerics). It includes Vreman's sub-grid scale model (Vreman 2004) and an ENO shock-capturing scheme, active only in regions marked by a shock sensor based on local dilatation and enstrophy (Ducros *et al.*

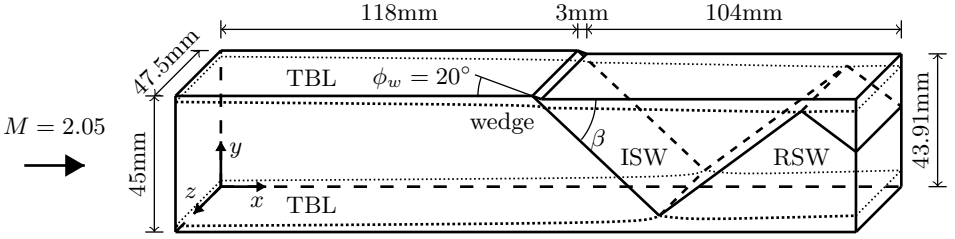

FIGURE 2. Computational setup and main flow features: M, Mach number; TBL, turbulent boundary layers (only top and bottom drawn, for clarity); ISW, incident shock wave; RSW, reflected shock waves; ϕ_w, wedge angle; β incident shock angle.

2000). In addition, an equilibrium wall model (Kawai & Larsson 2012) is used, which is described in some detail in subsection 2.1.

The mesh used for this simulation has nearly 30 million control volumes. The grid spacing is uniform in the stream-wise direction, with $\Delta x = 0.34$ mm $\approx \delta_0/16$. In the wall-normal directions ($\eta = y, z$), the grid is stretched over a length of $2\delta_0$ from each wall, with a geometric factor of seven and the grid spacing ranging from $\Delta\eta = 0.05$ mm $\approx \delta_0/108$ at the walls to an isotropic grid (i.e., $\Delta x = \Delta y = \Delta z$) in the central core. In viscous units: $(\Delta x^+, \Delta y^+, \Delta z^+) \approx (150, 22 \to 150 \to 22, 22 \to 150 \to 22)$. The resulting number of points per direction (x, y, z) is $(350+10+308) \times (67+70+67) \times (74+70+74)$.

2.1. *Wall-model*

Owing to the relatively high Reynolds number of the flow under consideration, the grid resolution near the wall is insufficient to resolve all the scales of the boundary layer, and the use of a wall-model is necessary. In the present simulation, the wall model proposed by Kawai & Larsson (2012) is used. It acts on a refined inner grid which is embedded in the coarser, outer LES grid (see Fig. 3). In the inner grid, the equilibrium-boundary-layer equations are solved:

$$\frac{\mathrm{d}}{\mathrm{d}\eta}\left[(\mu+\mu_t)\,\frac{\mathrm{d}u}{\mathrm{d}\eta}\right] = 0 \tag{2.1}$$

$$\frac{\mathrm{d}}{\mathrm{d}\eta}\left[(\mu+\mu_t)\,u\frac{\mathrm{d}u}{\mathrm{d}\eta} + c_p\left(\frac{\mu}{Pr}+\frac{\mu_t}{Pr_t}\right)\frac{\mathrm{d}T}{\mathrm{d}\eta}\right] = 0 \tag{2.2}$$

where η is the wall-normal coordinate, u is the velocity in the stream-wise direction, T is the temperature, c_p is the fluid-specific heat capacity at constant pressure, μ is the fluid molecular viscosity, Pr is the Prandtl number, Pr_t is the turbulent Prandtl number and μ_t is the eddy-viscosity, which is taken from a mixing-length model as

$$\mu_t = \kappa\rho\eta u_\tau\left[1-\exp\left(-\frac{\eta^+}{A^+}\right)\right]^2, A^+ = 17, \tag{2.3}$$

where $u_\tau \equiv \sqrt{\tau_w/\rho}$ is the friction velocity (characteristic velocity scale in a boundary layer with varying mean density, based on the wall shear stress, τ_w) and η^+ is the wall-normal coordinate normalized to viscous units, $\eta^+ \equiv \rho u_\tau \eta/\mu$. The model parameters are set constant: $\kappa = 0.41$, $Pr_t = 0.9$. A matching location is specified ($\eta = 0.05$ mm, or in wall units, $\eta^+ = 22$, in the present simulation), where the exchange of information between both grids/simulations occurs. The inner wall-model simulation takes the LES flow variables (ρ, u, T) at that location as its free-stream boundary condition (away from

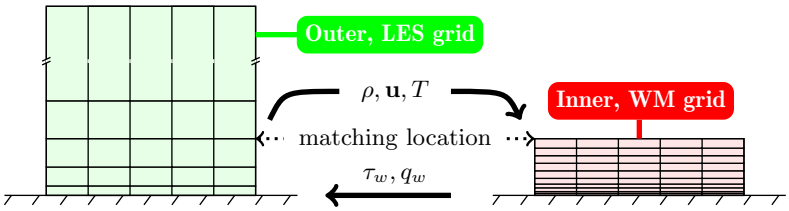

FIGURE 3. Wall-model schematic diagram.

the wall), whereas the outer LES takes the wall-shear stress and heat-flux at the wall, τ_w and q_w respectively, from the wall-model inner simulation. The wall-model is applied in all four walls of the LES, considered adiabatic to account for the long period over which the batches of PIV image pairs are gathered in the experiment.

2.2. *Turbulent inflow*

To avoid excessive computational cost, the computational domain comprises only part of the experimental setup. In particular, the domain does not include the converging/diverging nozzle and the initial part of the duct present in the experiment, where the boundary layers transition to turbulence. As a consequence, the boundary condition imposed at the inflow of the simulation must introduce not only mean velocity profiles but also suitable turbulence quantities that will account for the turbulent nature of the boundary layers, matching those extracted from the experiment. This is achieved by applying the synthetic method of turbulence generation proposed by Xie & Castro (2008), with the modifications of Touber & Sandham (2009), which is based on a digital filtering technique (see Klein *et al.* 2003) designed to match specified single- and two-point correlations. In our simulation, the generation of the turbulent inflow boundary condition is done in several steps:

(*a*) First, we use the 1D profiles measured in the experiment at a location 21 mm upstream of the foot of the wedge and in four xy-planes ($z = 2.5$, 4, 5.5 and 21 mm from one of the side walls) to generate 2D transverse-profiles for the mean and turbulent quantities corresponding to that measurement station. This is achieved by using symmetries, interpolation and constant extrapolation from the available experimental data.

(*b*) Because not all required mean/turbulent quantities are known from the experimental data, the 2D reconstructed profiles are used as the inflow to an independent wall-modeled LES of a constant-area duct with a 45.2 mm $\times$ 47.5 mm cross section that matches the inflow geometry of the final LES. Unknown turbulence quantities are initially set to zero and then let to evolve downstream until the turbulence is fully developed in the boundary layers. At that point, the complete set of 2D profiles for all required quantities is extracted from this additional duct-LES, time-averaged after the simulation has reached a statistically stationary state.

(*c*) Finally, to provide a boundary layer thickness in the final LES equivalent to the one measured experimentally at the station 21 mm upstream of the foot of the wedge ($\delta_0 = 5.4$ mm), the 2D profiles extracted from duct-LES at a downstream location in the computational domain are rescaled accordingly. The resulting profiles are then used as the inflow boundary condition to the LES simulating the experiment.

3. Results

This section presents a comparison of the LES results and the experimental measurements. The LES data were time-averaged over approximately 6.5 flow-through times (based on the center-line velocity magnitude), after an initial transient period. In this comparison we show first contour plots at four different xy-planes of mean and variances of the stream-wise and vertical velocity components, emphasizing the 3D effects that dominate this flow as we move closer to the side walls. Later, we focus on the interaction region between the incident and reflected shocks and the turbulent boundary layer of the bottom wall, by showing 1D mean velocity profiles (stream-wise, x, and vertical, y, components) extracted at several stream-wise locations near the shock-crossing point, in the $z = 21$ mm plane, both from the LES and the experiment. The presence of corner flows found in the LES is highlighted at the end of this section and their stream-wise evolution is qualitatively described.

3.1. *2D stream-wise/vertical mean and RMS velocity contours*

In the experiment, velocity data were acquired through high-resolution, 2D particle image velocimetry (PIV) at four xy planes located 2.5 mm, 4 mm, 5.5 mm and 21 mm from one of the side walls of the tunnel. The first three approximately span the boundary layer of such side wall, while the last plane is located near the center of the tunnel. They are thus targeted at exploring how 3D effects resulting from the presence of the side walls are translated into changes of the flow features. Details on the PIV setup and experimental data post-processing can be found in Helmer & Eaton (2011).

The same set of data was extracted from the LES and a comparison between experimental and simulation results is shown in Figs. 4-7. These figures focus on a region comprising both the wedge where the incident shock is generated off the top wall and the interaction and reflection on the turbulent boundary layer at the bottom wall.

The first observation that can be drawn from Figs. 4 and 5 is that there is a qualitative agreement between experiment and LES of the flow features in the mean stream-wise and vertical velocities and that the same trends are shown as we move to planes closer to the side walls. In particular, the shape of the thickened boundary layers near the wedge ($x \approx x_{wf} \equiv$ wedge foot location) and at the interaction ($x - x_{wf} \approx 45$ mm) seen in the stream-wise velocity (Fig. 4) is well captured by the simulation. Nevertheless, the thickness of the boundary layers appears smaller in the LES than in the experiment. This is confirmed when comparing the actual boundary layer thickness at the measurement station located 21 mm upstream of the foot of the wedge, where the LES shows a $\delta_0 \approx 5.0$ mm, almost 10% smaller than in the experiment.

In the experiment it was found that the shock angle resulting from the small 20° wedge was $\beta \approx 37°$, significantly lower than the 52° predicted by inviscid theory. In the LES, an angle of approximately 39° is found. A smaller incoming boundary thickness in the simulation, as previously described, could be responsible for the higher shock angle found in the LES, when compared with that in the experiment, because viscous effects would affect a smaller region of the flow, bringing the value of that angle slightly closer to the one predicted by inviscid theory.

From the comparison of the vertical velocity contours (Fig. 5) it is observed first that the influence of the wedge extends slightly more upstream in the simulation than in the experiment. At the interaction, the regions found in the experiment in the $z = 21$ mm plane of high and low negative vertical velocity to the left and right, respectively, of the crossing point between incident and reflected shocks are also reproduced in the LES,

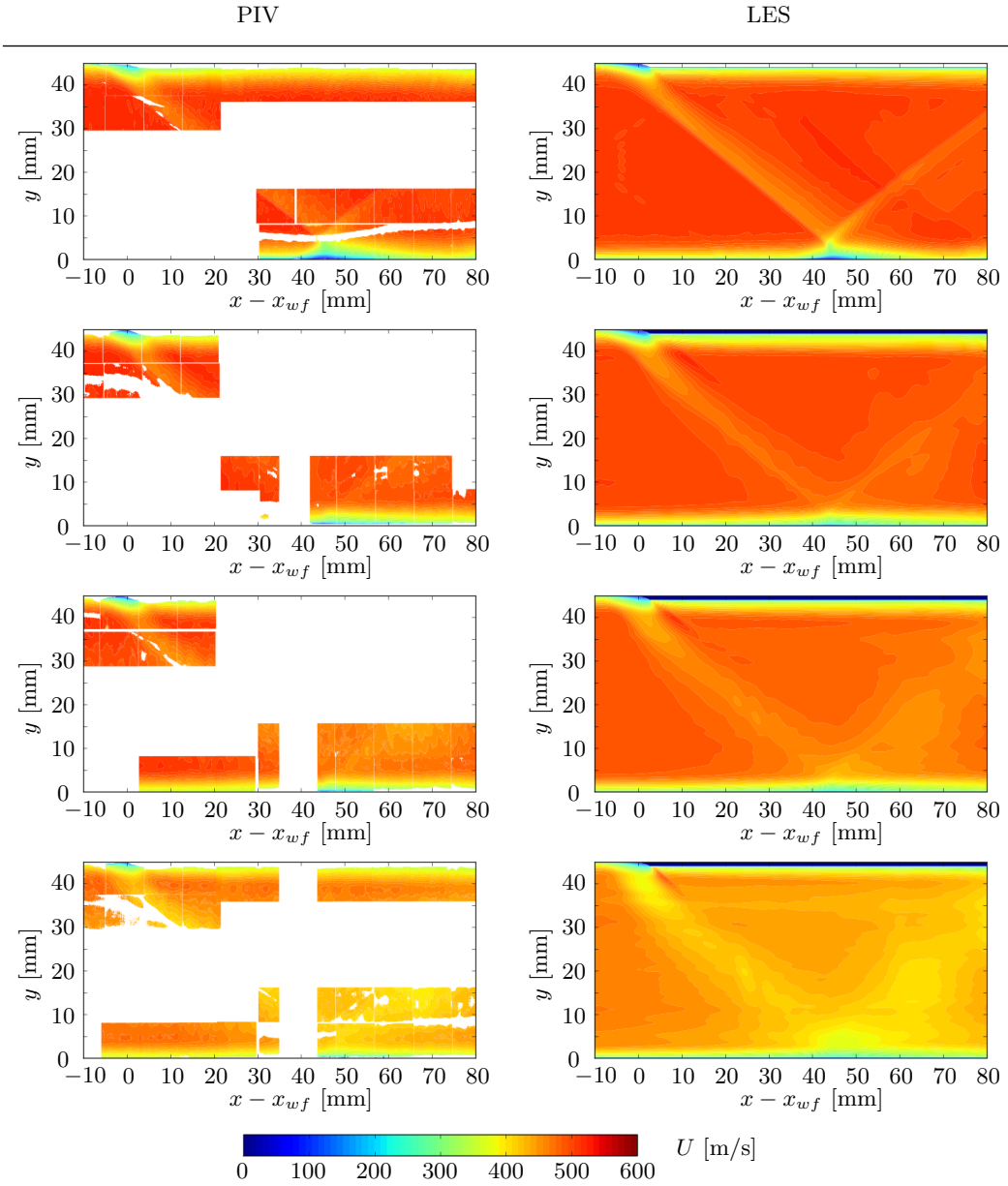

FIGURE 4. Mean stream-wise velocity contours at span-wise-normal planes located 21, 5.5, 4 and 2.5 mm (top to bottom, respectively) from one of the side walls, obtained from PIV (left) and LES (right). Experimental data in white regions on the left plots could not be collected.

although there are some differences in the shape of those regions. Notice that the higher shock angle found in the LES brings the shock-crossing point and those high/low-vertical-velocity regions to a location slightly more upstream than in the experiment. Also, the positive vertical velocity regions found in the experiment immediately downstream of the shock in the vicinity of the wedge for the $z = 5.5$ and 4 mm planes are also reproduced in the LES, which also shows such a region (although more confined near the wedge) for

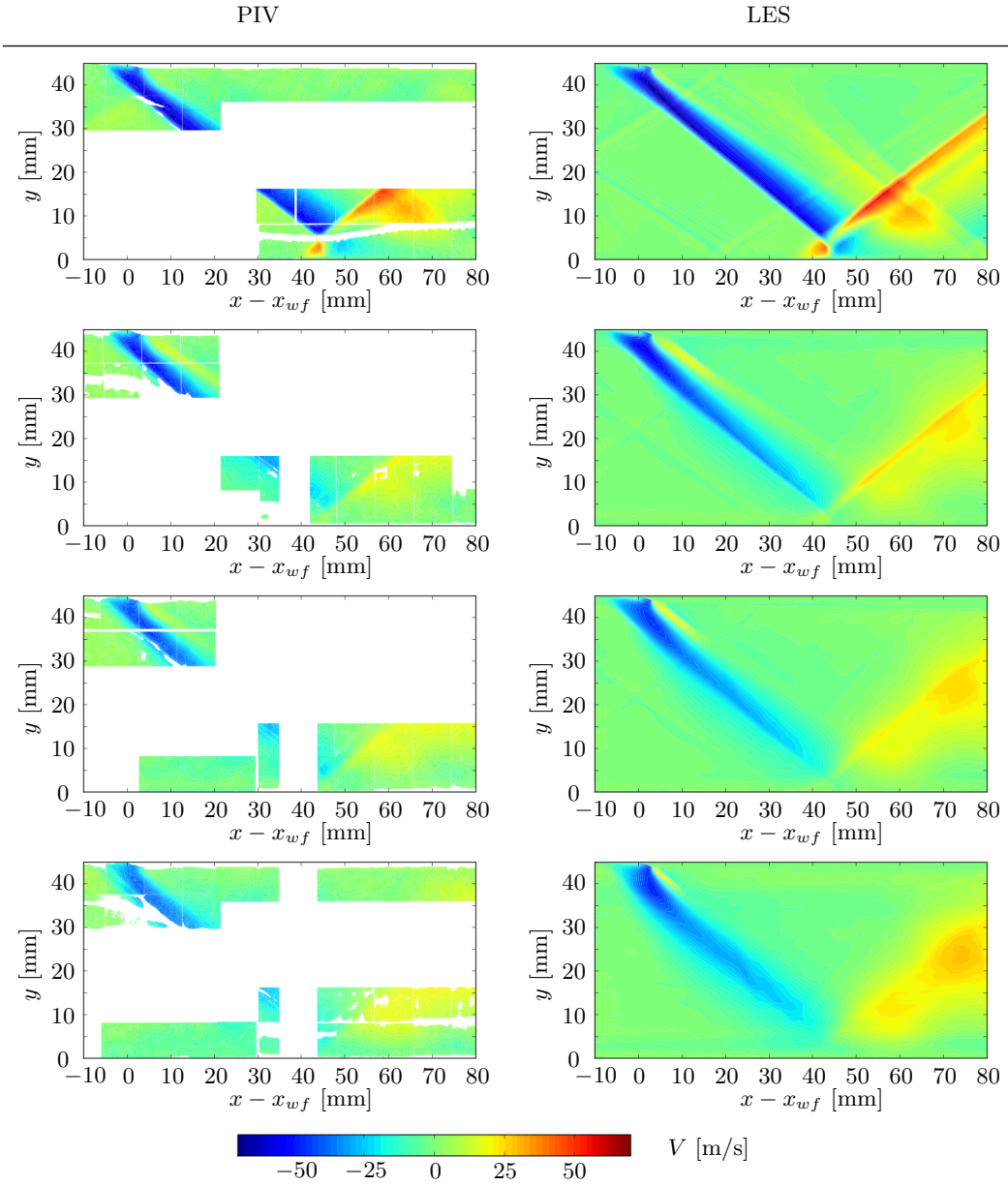

FIGURE 5. Mean vertical velocity contours at span-wise-normal planes located 21, 5.5, 4 and 2.5 mm (top to bottom, respectively) from one of the side walls, obtained from PIV (left) and LES (right). Experimental data in white regions on the left plots could not be collected.

the $z = 2.5$ mm plane, although not observable in the experimental data. The $z = 5.5$ mm plane shows a reflected shock that is somewhat sharper in the LES than in the experiment, also reaching higher values of the mean vertical velocity.

When examining turbulence quantities (see Figs. 6 and 7) we noted that, whereas a general agreement is observed between experiment and LES, the differences are more noticeable than in the mean quantities. In particular, the extent near the top and bottom

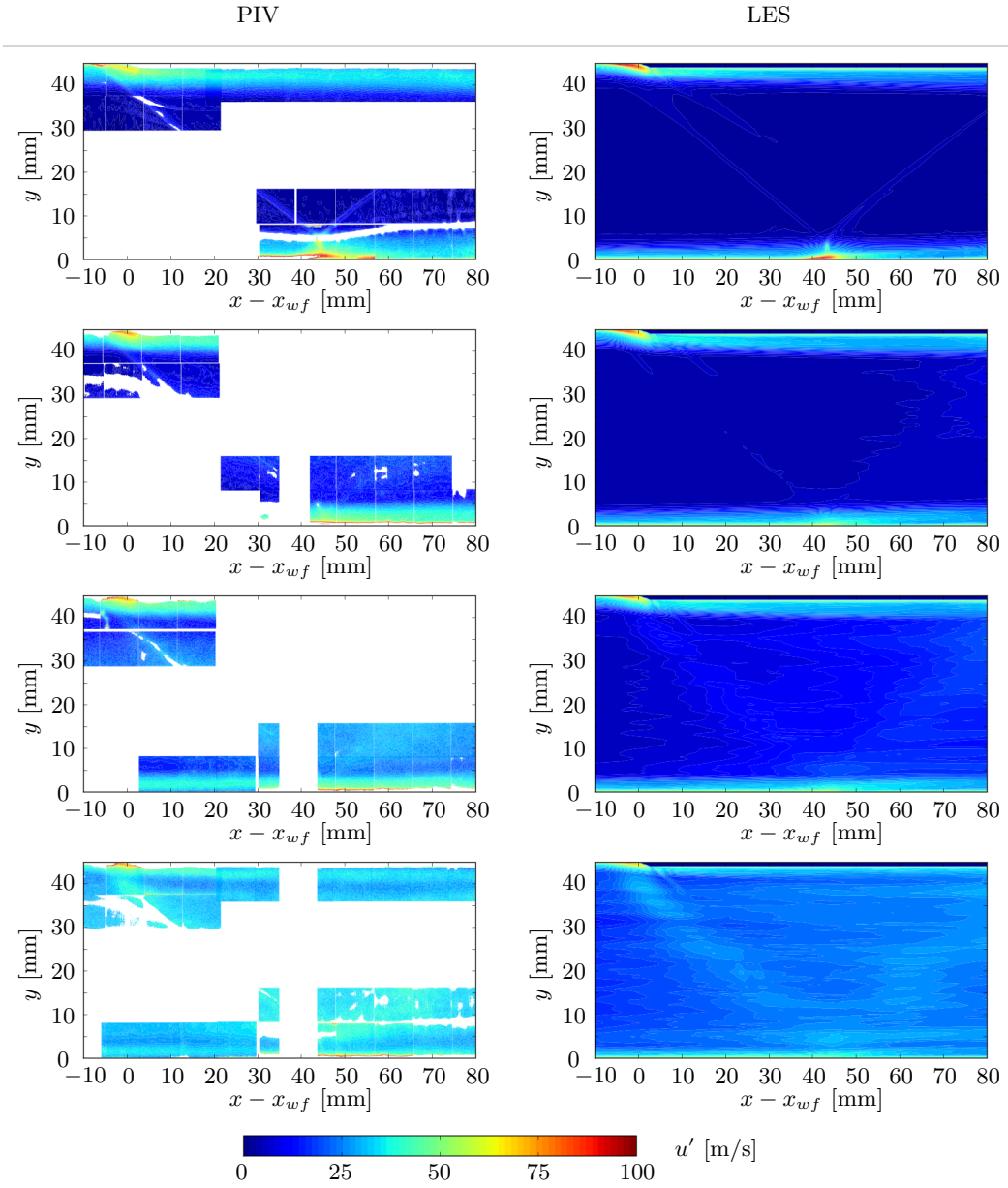

FIGURE 6. RMS stream-wise velocity contours at span-wise-normal planes located 21, 5.5, 4 and 2.5 mm (top to bottom, respectively) from one of the side walls, obtained from PIV (left) and LES (right). Experimental data in white regions on the left plots could not be collected.

walls where turbulent intensity is significant appears smaller in the simulation than in the experiment. This is consistent with the previous observation of a thinner boundary layer thickness upstream of the wedge foot for the LES, but other sources of discrepancy are being investigated (for example, a different shape of the wall-normal profiles of such RMS quantities resulting from different development of the turbulent boundary layers). Thinner boundary layers would also occur at the side walls and explain the lower values of

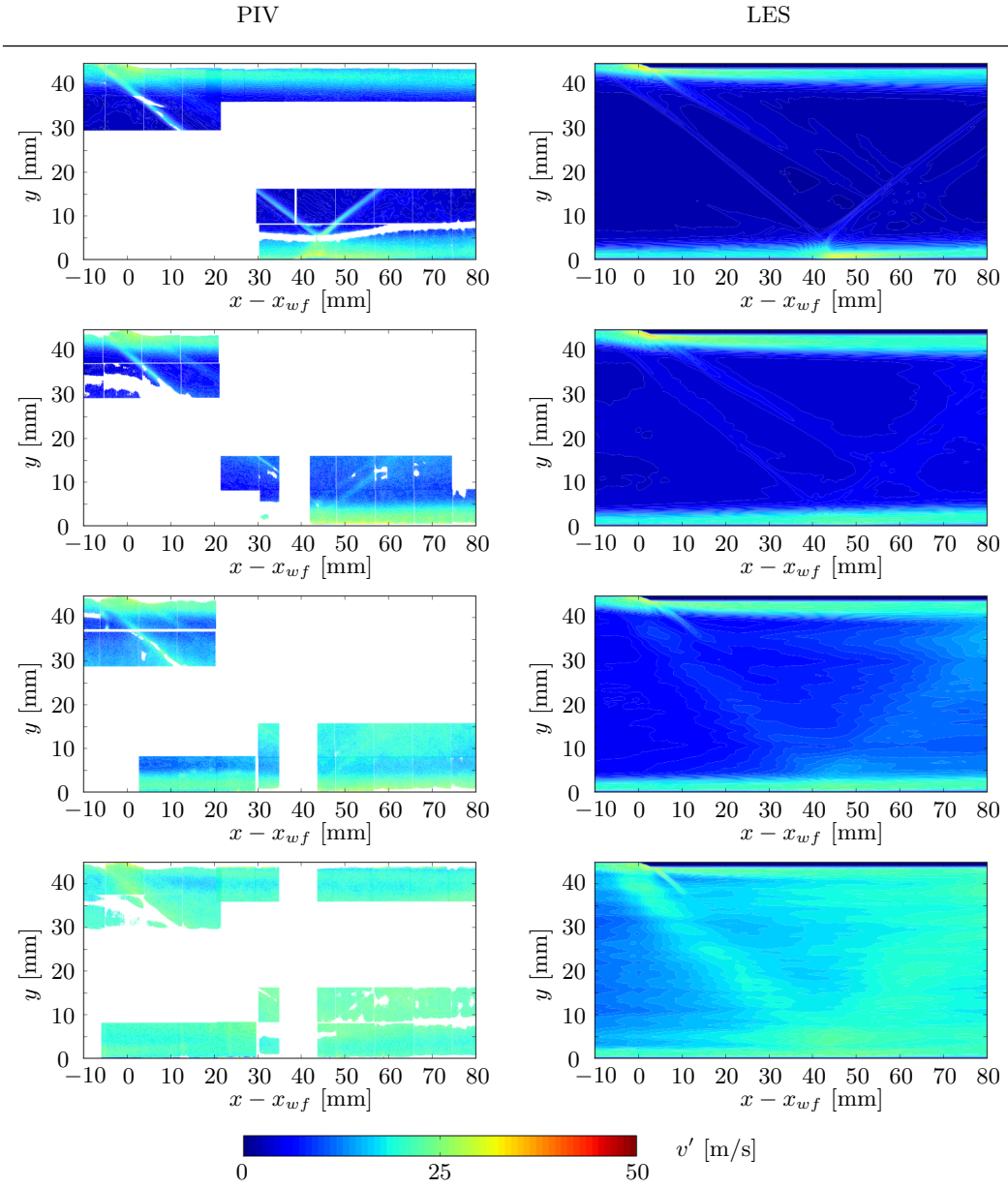

FIGURE 7. RMS vertical velocity contours at span-wise-normal planes located 21, 5.5, 4 and 2.5 mm (top to bottom, respectively) from one of the side walls, obtained from PIV (left) and LES (right). Experimental data in white regions on the left plots could not be collected.

turbulent intensity found in the simulation for planes near the side wall ($z = 2.5, 4$ mm), when compared with that of the experiment. The lower values of RMS vertical velocity found in the simulation for the incident and reflected shock waves may be a consequence of the dissipative nature of the shock-capturing numerical method in use (consistent with the theoretical prediction of Larsson 2010).

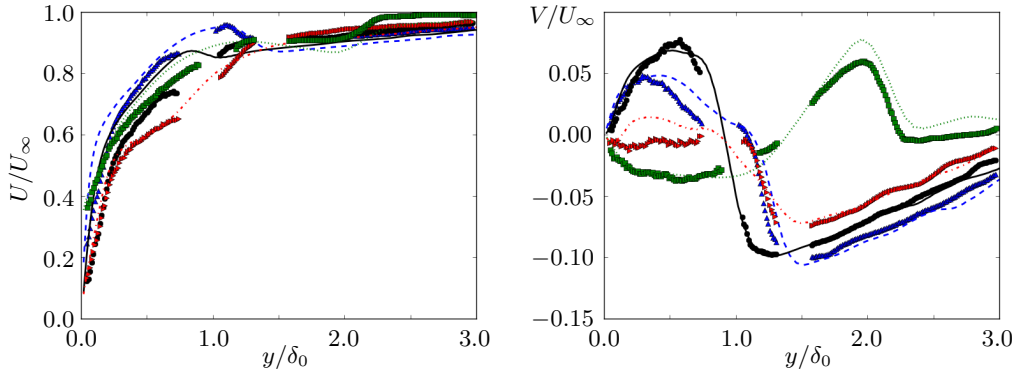

FIGURE 8. Mean stream-wise (left) and vertical (right) velocity profiles in the vertical direction, y, extracted from PIV (markers) and LES (lines) on the span-wise normal plane located at $z = 21$ mm, for several stream-wise locations (-2, 0, 2, 8 mm), relative to the shock-crossing point. Wall-normal coordinate is normalized by the boundary layer thickness, δ_0, at a location 21 mm upstream of the foot of the wedge in the $z = 21$ mm plane in the experiment and simulation. Lines represent LES results (dashed: x = -2 mm, continuous: $x = 0$ mm, dashed-dotted: $x = 2$ mm, dotted: $x = 8$ mm) and markers represent PIV results (up-triangles: x = -2 mm, circles: $x = 0$ mm, right-triangles: $x = 2$ mm, squares: $x = 8$ mm).

3.2. *Wall-normal 1D mean velocity profiles at the interaction*

We focus our attention now on the interaction region between the incident/reflected shocks and the turbulent boundary layer at the bottom wall. Fig. 8 shows 1D profiles of the mean stream-wise and vertical velocity components in the $z = 21$ mm plane, at stream-wise locations $x - x_{SC} = -2, 0, 2, 8$ mm, where x_{SC} is the shock-crossing point (see Fig. 1). The wall-normal coordinate, y, in those plots has been normalized with the boundary layer thickness found at the measurement station located 21 mm upstream of the foot of the wedge, δ_0, with corresponding values of 5.4 mm for the experiment and 5.0 mm for the LES.

The mean stream-wise velocity profiles extracted from the simulation reflect qualitatively the shapes and trends observed in the experiment. For example, the fuller profile inside the boundary layer observed for the location 2 mm upstream of the shock-crossing point (dashed line) followed by the deceleration at $y/\delta_0 \approx 1.2$ and the subsequent slow increase in speed away from the wall is well captured in the simulation. Similarly, changes in the slopes of the profiles 2 and 8 mm downstream of the shock-crossing point (dash-dotted and dotted curves, respectively) agree with the experimental results. Nevertheless, quantitatively it is seen that the simulation shows a consistent over-prediction of the experimental values inside the boundary layer ($y/\delta_0 \lesssim 1$) and an under-prediction outside the boundary layer ($y/\delta_0 \gtrsim 1$). These discrepancies might be the result of a different development of the incoming turbulent boundary layer between experiment and simulation and are presently under investigation.

For the mean vertical velocity, the stream-wise evolution of these profiles is well-captured, showing profile shapes in good agreement with the experiment. The profiles at $x = x_{SC}$ are almost identical. Profiles 2 mm upstream and downstream of the shock-crossing point (dashed and dash-dotted lines, respectively) also show good agreement for $y > \delta_0$, whereas inside the boundary layer, the simulation over-predicts the values observed in the experiment. Further downstream, the opposite holds: the agreement inside

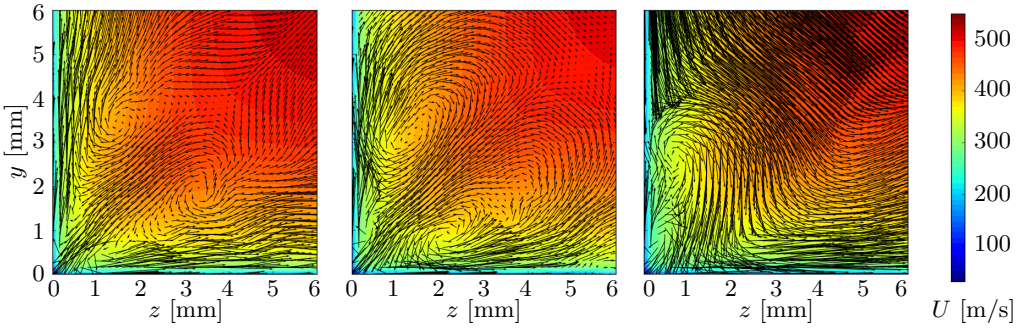

(a) $x - x_{wf} = -21$ mm (b) $x - x_{wf} = 11$ mm (b) $x - x_{wf} = 28$ mm

FIGURE 9. Downstream evolution (from LES) of corner flow in the vicinity of $y = z = 0$, for stream-wise locations (relative to the wedge foot): $x - x_{wf}$ =-21, 11 and 28 mm (from left to right). Contours of mean stream-wise velocity, U, are superimposed with arrows representing the transverse velocity, $V\mathbf{e}_y + W\mathbf{e}_z$, where $\mathbf{e}_\alpha$ is the versor in the α-coordinate direction.

the boundary layer is good but there is an over-prediction outside. Even then, the shape of these profiles is remarkably close to the experimental data.

3.3. *Corner flows*

An important consequence of the three-dimensionality of the the flow brought in by the side walls in combination with the presence of turbulent boundary layers is the generation of secondary flows of Prandtl's second kind, referred to in Bradshaw (1987) as "stress-induced secondary flows", since the gradients of Reynolds stresses produce the stream-wise mean vorticity responsible for such secondary flows. Theoretical, experimental and numerical studies (Gessner 1973; Gessner *et al.* 1987; Davis *et al.* 1986; Joung *et al.* 2007) have investigated these corner flows occurring in ducts, both in subsonic and supersonic turbulent flow conditions. Nevertheless, the presence of shocks and how they affect the evolution of such corner flows has received less attention and it is targeted in our present work. No experimental data were available from Helmer & Eaton (2011) to contrast with the simulation results, so the following observations are lacking experimental validation and should be taken with care.

Fig. 9 shows contours of mean stream-wise velocity magnitude obtained from the numerical simulation in the vicinity of the $y = z = 0$ corner (bottom left corner, when looking downstream) at three different transverse planes upstream of the interaction region, with the transverse velocity vector field superimposed. The first plot corresponds to a location 21 mm upstream of the foot of the wedge, thus unaffected by the incident shock, and clearly shows that the wall-modeled LES is able to reproduce such corner flows. Two counter-rotating vortices are noticed at this stream-wise location, which are almost symmetrical with respect to the $y = z$ line. A moderately strong flow is produced along this line and directed toward the corner. Note that the vortices are inside the boundary layer ($\delta_0 \approx 5.0$ at this stream-wise location).

As we move downstream (center plot), the downwash generated by the incident shock breaks the symmetry of the corner flow configuration. Notice in Fig. 5 how the region of negative mean vertical velocity that distinguishes the incident shock spreads out near the side wall (bottom plots), compared with the $z = 21$ mm plane located away from the side walls (top plot), for which the incident shock is more sharply defined and has a minimal influence on the bottom boundary layer for that streamwise location of $x - x_{wf} = 11$

mm. As a consequence, the upper vortex, closer to the side wall, is slightly pushed down and closer to the side wall, despite the growth in the boundary layer (observable in the background mean stream-wise velocity contours) with the flow pattern around it becoming ellipsoidal. The shape of the lower vortex, closer to the bottom wall, is also affected and appears to split into a nested pair of co-rotating vortices, also ellipsoidal. Moving even farther downstream (right plot), the strong downward component of the transverse velocity is evident in the top part of the plot. The upper vortex has moved much closer to the side wall, whereas the bottom vortex has disappeared and the flow pattern is no longer directed toward the corner along the line $y = z = 0$, but almost directly downward and then away from the side wall.

4. Conclusions and future work

A wall-modeled large-eddy simulation has been performed with the aim to reproduce the experimental results by Helmer & Eaton (2011) of a $M = 2.05$ shock-turbulent-boundary-layer interaction in a low-aspect ratio duct. In addition to studying the suitability of wall-modeled LES for an accurate prediction of flow features of the interaction near the center of the duct, this work also targets the study of 3D effects caused by the presence of the side walls, which were investigated in detail in the experiment.

Mean and turbulent quantities were compared between the experiment and simulation at four different planes parallel to the side walls. The flow features of the interaction and the 3D effects appear qualitatively well captured by the simulation, reflecting the spread out of mean and turbulent quantities when nearing the side walls, consistent with the experimental results. The experimental value of the shock-angle of the incident shock, which is generated by a small wedge located on the top wall of the duct was recovered within 5% by the simulation. The discrepancy may be caused by thinner boundary layers resulting from the LES, compared with that seen in the experiment, which would have the effect of bringing the value of the shock angle somewhat closer to the one predicted by inviscid theory. Two-dimensional contour plots of Reynolds stresses also show thinner boundary layers in the simulation that differ in shape from the experiment. A possible explanation could be a different level of turbulent development. Despite these discrepancies, 1D profiles of mean stream-wise and wall-normal velocities in the simulation, properly rescaled to account for different boundary layer thicknesses, predict the same trends as those of the experiment.

Three-dimensional effects are further manifested by the presence of corner flows, which are qualitatively investigated in this brief, as they evolve from a streamwise location that can be considered free of any shock influence toward downstream locations where the downward motion of the incident shock is felt near the corner. The initially symmetric pair of counter-rotating vortices is pushed closer to the bottom and side walls by the action of the spread-out shock. One of the vortices is transformed into a set of two co-rotating vortices near the bottom wall before it is eventually washed out by the action of the downward vertical velocity induced by the shock, breaking the symmetry of the vortex pair. This scenario has not been directly validated with experimental or DNS results, so the conclusions must be taken as mere observations extracted from the present simulation. Nonetheless, the ability of the wall-modeled LES to reproduce these corner flows is encouraging to pursue as further analysis in the future.

More validation steps are necessary, including an assessment of grid-resolution independence of these results, as well as a systematic evaluation of the influence of time-

averaging period used to collect statistics. The effect of different matching locations utilized in the wall-model should also be studied, focusing particularly on how shock-free, shock-interaction and corner regions might be affected by such a parameter. Ensuring a better match with the experiment for the incoming boundary layers (both thickness and turbulent development) is currently being addressed. Finally, new simulations are planned with a modified geometry that includes a 3 mm-high wedge to study the case of shock-turbulent-boundary-layer interaction with flow separation.

Acknowledgments

Financial support has been provided by the United States Department of Energy under the Predictive Science Academic Alliance Program (PSAAP) at Stanford University. The authors are grateful to Dr. Joseph W. Nichols for his valuable comments and remarks on a preliminary version of this manuscript. The authors acknowledge the following award for providing computing resources that have contributed to the research results reported in this brief: "MRI-R2: Acquisition of a Hybrid CPU/GPU and Visualization Cluster for Multidisciplinary Studies in Transport Physics with Uncertainty Quantification" `http://www.nsf.gov/awardsearch/showAward.do?AwardNumber=0960306`. This award is funded under the American Recovery and Reinvestment Act of 2009 (Public Law 111-5).

REFERENCES

Bradshaw, P. 1987 Turbulent secondary flows. *Annu. Rev. Fluid Mech.* **19**, 53–74.

Davis, D. O., Gessner, F. B. & Kerlick, G. D. 1986 Experimental and numerical investigation of supersonic turbulent flow through a square duct. *AIAA J.* **24** (1508).

Dolling, D. S. 2001 Fifty years of shock-wave/boundary-layer interaction research: what next? *AIAA J.* **39**, 1517.

Ducros, F., Laporte, F., Souleres, T. & Guinot, V. 2000 High-order fluxes for conservative skew-symmetric-like schemes in structures meshes: Application to compressible flows. *J. Comput. Phys.* **161**, 114.

Dupont, P., Haddad, C. & Debiève, J. 2006 Space and time organization in a shock-induced separated boundary layer. *J. Fluid. Mech* **559**, 255–277.

Dupont, P., Piponniau, S., Sidorenko, A. & Debive, J. 2008 Investigation by particle image velocimetry measurements of oblique shock reflection with separation. *AIAA J.* **48** (6), 1365–1370.

Garnier, E., Sagaut, P. & Deville, M. 2002 Large eddy simulation of shock/boundary-layer interaction. *AIAA J.* **40** (10).

Gessner, F. B. 1973 The origin of secondary flow in turbulent flow along a corner. *J. Fluid Mech.* **58**, 1–25.

Gessner, F. B., Ferguson, S. D. & Lo, C. H. 1987 Experiments on supersonic turbulent flow development in a square duct. *AIAA J.* **25** (690).

Hadjadj, A., Larsson, J., Morgan, B. E., Nichols, J. W. & Lele, S. K. 2010 Large-eddy simulation of shock/boundary-layer interaction. *Annu. Res. Briefs* pp. 141–152.

Helmer, D. & Eaton, J. 2011 Measurements of a three-dimensional shock-boundary layer interaction. *Tech. Rep.* TF-126. Flow Physics and Computational Engineering Group, Department of Mechanical Engineering, Stanford University.

Humble, R., Elsinga, G., Scarano, F. & van Oudheusden, B. 2009 Three-dimensional instantaneous structure of a shock wave/turbulent boundary layer interaction. *J. of Fluid Mech.* **622**, 33–62.

Joung, Y., Choi, S. U. & Choi, J.-I. 2007 Direct numerical simulation of turbulent flow in a square duct: Analysis of secondary flows. *J. Eng. Mech.* **213**, 213–221.

Kawai, S. & Larsson, J. 2012 Wall-modeling in large eddy simulation: length scales, grid resolution and accuracy. *Phys. Fluids* (to appear).

Khalighi, Y., Nichols, J. W., Lele, S., Ham, F. & Moin, P. 2011 Unstructured large eddy simulations for prediction of noise issued from turbulent jets in various configurations. *AIAA* **2886**.

Klein, M., Sadiki, A. & Janicka, J. 2003 A digital filter based generation of inflow data for spatially developing direct numerical or large eddy simulations. *J. Comput. Phys.* **186**, 652–665.

Larsson, J. 2010 Effect of shock-capturing errors on turbulence statistics. *AIAA J.* **48** (7), 1554–1557.

Pirozzoli, S. & Grasso, F. 2006 Direct numerical simulation of impinging shock wave/turbulent boundary layer interaction at m = 2.25. *J. Comput. Phys.* **18** (6), 065113–1–17.

Pirozzoli, S., Larsson, J., Nichols, J. W., Bernardini, M., Morgan, B. E. & Lele, S. K. 2010 Analysis of unsteady effects in shock/boundary layer interactions. *Annu. Res. Briefs* pp. 153–164.

Souverein, L., Dupont, P., Debieve, J., van Dussaugen, J., Oudheusden, B. & Scarano, F. 2010 Effect of interaction strength on unsteadiness in turbulent shock-wave-induced separations. *AIAA J.* **48**, 1480–1493.

Touber, E. & Sandham, N. 2009 Large-eddy simulation of low-frequency unsteadiness in a turbulent shock-induced separation bubble. *Theor. Comput. Fluid Dyn.* **23**, 79–107.

Vreman, A. W. 2004 An eddy-viscosity subgrid-scale model for turbulent shear flow: Algebraic theory and applications. *Phys. Fluids* **16** (10), 3670–3681.

Wu, M. & Martin, M. 2008 Analysis of shockmotion in shockwave and turbulent boundary layer interaction using direct numerical simulation data. *J. Fluid Mech.* **594**, 71–83.

Xie, Z.-T. & Castro, I. P. 2008 Efficient generation of inflow conditions for large eddy simulation of street-scale flows. *Flow Turbul. Combust.* **81** (3), 449–470.